A&A 570, A60 (2014)
DOI: 10.1051/0004-6361/201424495

Astronomy & Astrophysics

The LOFAR pilot surveys for pulsars and fast radio transients⋆

Thijs Coenen[1,2], Joeri van Leeuwen[2,1], Jason W. T. Hessels[2,1], Ben W. Stappers[3], Vladislav I. Kondratiev[2,4], A. Alexov[1,5], R. P. Breton[6], A. Bilous[7], S. Cooper[3], H. Falcke[7,2], R. A. Fallows[2], V. Gajjar[8,3], J.-M. Grießmeier[9,10], T. E. Hassall[6], A. Karastergiou[11], E. F. Keane[12,13], M. Kramer[14,3], M. Kuniyoshi[14], A. Noutsos[14], S. Osłowski[14,15], M. Pilia[2], M. Serylak[11], C. Schrijvers[16], C. Sobey[2], S. ter Veen[7], J. Verbiest[15], P. Weltevrede[3], S. Wijnholds[2], K. Zagkouris[11], A.S. van Amesfoort[2], J. Anderson[17,18], A. Asgekar[2,19], I. M. Avruch[20,21], M. E. Bell[22], M. J. Bentum[2,23], G. Bernardi[24], P. Best[25], A. Bonafede[26], F. Breitling[18], J. Broderick[6], M. Brüggen[26], H. R. Butcher[27], B. Ciardi[28], A. Corstanje[7], A. Deller[2], S. Duscha[2], J. Eislöffel[29], R. Fender[11], C. Ferrari[30], W. Frieswijk[2], M. A. Garrett[2,31], F. de Gasperin[26], E. de Geus[2,32], A. W. Gunst[2], J. P. Hamaker[2], G. Heald[2], M. Hoeft[29], A. van der Horst[1], E. Juette[33], G. Kuper[2], C. Law[34,1], G. Mann[18], R. McFadden[2], D. McKay-Bukowski[35,36], J. P. McKean[2,21], H. Munk[2], E. Orru[2], H. Paas[37], M. Pandey-Pommier[38], A. G. Polatidis[2], W. Reich[14], A. Renting[2], H. Röttgering[31], A. Rowlinson[1], A. M. M. Scaife[6], D. Schwarz[15], J. Sluman[2], O. Smirnov[39,40], J. Swinbank[1], M. Tagger[9], Y. Tang[2], C. Tasse[41], S. Thoudam[7], C. Toribio[2], R. Vermeulen[2], C. Vocks[18], R. J. van Weeren[24], O. Wucknitz[14], P. Zarka[41], and A. Zensus[14]

(Affiliations can be found after the references)

Received 28 June 2014 / Accepted 1 August 2014

ABSTRACT

We have conducted two pilot surveys for radio pulsars and fast transients with the Low-Frequency Array (LOFAR) around 140 MHz and here report on the first low-frequency fast-radio burst limit and the discovery of two new pulsars. The first survey, the LOFAR Pilot Pulsar Survey (LPPS), observed a large fraction of the northern sky, $\sim 1.4 \times 10^4$ deg^2, with 1 h dwell times. Each observation covered $\sim$75 deg^2 using 7 independent fields formed by incoherently summing the high-band antenna fields. The second pilot survey, the LOFAR Tied-Array Survey (LOTAS), spanned $\sim$600 deg^2, with roughly a 5-fold increase in sensitivity compared with LPPS. Using a coherent sum of the 6 LOFAR "Superterp" stations, we formed 19 tied-array beams, together covering 4 deg^2 per pointing. From LPPS we derive a limit on the occurrence, at 142 MHz, of dispersed radio bursts of <150 day^{-1} sky^{-1}, for bursts brighter than $S > 107$ Jy for the narrowest searched burst duration of 0.66 ms. In LPPS, we re-detected 65 previously known pulsars. LOTAS discovered two pulsars, the first with LOFAR or any digital aperture array. LOTAS also re-detected 27 previously known pulsars. These pilot studies show that LOFAR can efficiently carry out all-sky surveys for pulsars and fast transients, and they set the stage for further surveying efforts using LOFAR and the planned low-frequency component of the Square Kilometer Array.

Key words. pulsars: general – telescopes – surveys

1. Introduction

The Low-Frequency Array (LOFAR; van Haarlem et al. 2013), with its high sensitivity and flexible observing configurations, is set to open the lowest radio frequencies to efficient pulsar surveys. Its operating frequency of 10−240 MHz means a return to the long-wavelength range at which pulsars were originally discovered. The first pulsars were detected at 81.5 MHz, with the Cambridge Inter Planetary Scattering array (Hewish et al. 1968). Since then, however, most pulsar surveys have avoided low radio frequencies (<300 MHz) because of a number of effects that scale strongly with decreasing frequency and severely affect pulsar detectability (Stappers et al. 2011). First, at low frequencies, dispersion correction requires many more, narrower frequency channels (Lorimer & Kramer 2005), and searches need a much finer grid of trial dispersion measures (DMs). Second, multi-path propagation caused by interstellar scattering broadens the intrinsically short duration pulses, scaling with frequency ν as $\nu^{-3.9}$ (Bhat et al. 2004). Lastly, the sky background temperature $T_{\rm sky}$ increases at low frequencies as $\nu^{-2.6}$ (Lawson et al. 1987).

These drawbacks are partially compensated for by the steep pulsar spectral indices, $S \propto \nu^{-1.8}$ on average (Maron et al. 2000; interpreted further in Bates et al. 2013), with outliers of $S \propto \nu^{-2} - \nu^{-4}$ (Hassall et al., in prep.). Furthermore, as many pulsar spectra turn over toward lower frequencies, flux densities typically peak in the 100–200 MHz band (Malofeev et al. 2000; Hassall et al., in prep.). Finally, for some pulsars only the wider, low-frequency beam may cross Earth (Stappers et al. 2011). Overall these make a compelling low-frequency search case.

A number of low-frequency surveys have recently been performed between 16 and 400 MHz: The Ukrainian UTR-2 radio telescope carried out a pulsar census in the 16.5−33.0 MHz band (Zakharenko et al. 2013). A 34.5-MHz pulsar survey undertaken with the Gauribidanur telescope resulted in the first (potential) radio detection of *Fermi* pulsar J1732−3131 (Maan et al. 2012) – a source that might only be detectable below 50 MHz. The Cambridge array performed a second pulsar survey at 81.5 MHz but did not discover any new pulsars

⋆ http://www.astron.nl/pulsars/lofar/surveys/lotas/

(Shrauner et al. 1998). The ongoing Arecibo drift survey for pulsars at 327 MHz discovered 24 new pulsars (Deneva et al. 2013). A survey of the Cygnus region using the Westerbork Synthesis Radio Telescope (WSRT) at 328 MHz led to the discovery of 3 new pulsars (Janssen et al. 2009), also demonstrating the use of a dish-based radio interferometer for pulsar searching. Perhaps most importantly, several 300–400 MHz surveys have recently been conducted using the Green Bank Telescope (GBT). Through their high time and frequency resolution, these surveys have discovered over 100 normal and millisecond pulsars so far (Hessels et al. 2008; Boyles et al. 2013; Lynch et al. 2013; Stovall et al. 2014).

Low-frequency surveys can also achieve large instantaneous sky coverage and sensitivity. That is important, as over the last decade it has become increasingly apparent that the various subtypes of radio-emitting neutron stars show a wide range of activity – from the classical, steady pulsars to the sporadic pulses of the rotating radio transients (RRATs; McLaughlin et al. 2006), and the off-on intermittent pulsars (Kramer et al. 2006). Other cases of transient millisecond radio pulsars (Archibald et al. 2009; Papitto et al. 2013; Bassa et al. 2014; Stappers et al. 2014) and radio magnetars (Camilo et al. 2006; Eatough et al. 2013) also give strong motivation for pulsar surveys that permit large on-sky time and repeated observations of the same survey area. Furthermore, the recent discovery of the fast radio bursts (FRBs, also known as "Lorimer bursts"; Lorimer et al. 2007; Keane et al. 2012; Thornton et al. 2013; Spitler et al. 2014; Petroff et al. 2014) provides even more impetus for wide-field radio surveys with sub-millisecond time resolution.

LOFAR operates in two observing bands by using two different types of antennas: the LOFAR low-band antennas (LBA; 10−90 MHz) and the LOFAR high-band antennas (HBA; 110−240 MHz), which together cover the lowest 4 octaves of the radio window observable from Earth. It has a dense central core in the north of the Netherlands. Core HBA stations consist of two identically sized "sub-stations" (Fig. 4 in van Haarlem et al. 2013). LOFAR uses digital electronics and high-speed fiber networks to create a low-frequency interferometric array that is more versatile and scientifically capable than its predecessors. In particular, through the use of multi-beaming techniques LOFAR can achieve very large (tens of square degrees) fields-of-view, which are ideal for performing efficient pulsar and fast transient surveys. The wide fractional bandwidth and capability to store and process hundreds of terabytes of high-resolution data make it an even more powerful instrument. A general overview of LOFAR's pulsar observing capabilities is provided in Stappers et al. (2011), while LOFAR pulsar-survey strategies are outlined and simulated in van Leeuwen & Stappers (2010).

During the 2008–2012 commissioning of LOFAR, we performed two pilot pulsar surveys. Efficient pulsar surveys ideally combine high sensitivity, a large total field-of-view (FoV) and a high angular resolution per FoV element. LOFAR's beam-formed modes (Stappers et al. 2011) can form up to hundreds of beams simultaneously (Romein et al. 2010), and thus provide such a wide view (>10 deg^2) as well as the ability to constrain positions to a few arcminutes. The first survey, employing *incoherent* beam-forming, is called the LOFAR Pilot Pulsar Survey (LPPS; Fig. 1, left panel), while the second survey, the LOFAR Tied-Array Survey (LOTAS; Fig. 1, middle panel) employed *coherent* or tied-array beam forming. Incoherent beam-forming (Backer 2000) provides lower raw sensitivity, with pulsar signal-to-noise (S/N) increasing only as the square root of the number of stations being added. But it does allow one to observe bright, rare events because of its large FoV, clear from

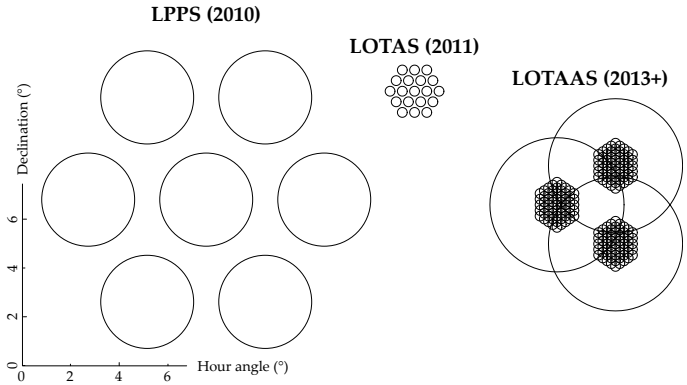

Fig. 1. Single-pointing footprints of LPPS (*left*) and LOTAS (*middle*). Circles denote the half-power beam widths at the respective central frequencies (Table 1). For comparison (*right*) is the single-pointing footprint of the ongoing LOFAR Tied-array All-sky Survey LOTAAS (Sect. 5). The LOTAAS pointings use both incoherent (large circles) and coherent (clusters of small circles) beams.

Fig. 1. Coherent beam-forming, in contrast, permits maximum instantaneous sensitivity, scaling linearly with the number of stations summed. The resulting tied-array beams have limited FoV, however, scaling as the inverse of the maximum distance between stations (Stappers et al. 2011).

In this paper, we present the setup of these two surveys (Sects. 2 and 3). In Sect. 4 we then report on the new and known pulsars that were detected and present limits for the rate of fast radio transients in general. Section 5 contains overall conclusions, and looks forward to currently ongoing and future work. Profiles and parameters for the detected and discovered pulsars can be found in Appendices A and B. These sections are all described in greater detail in Coenen (2013, henceforth C13), and throughout this paper we will refer the interested reader to specific sections of C13.

2. Observations

In LPPS we *incoherently* added as many LOFAR stations as were available; For LOTAS we only *coherently* combined stations from the 300-m-wide LOFAR "Superterp", which has a much higher filling factor (Backer 2000; van Leeuwen & Stappers 2010) than the rest of the array (Table 1).

2.1. LPPS survey

The LPPS survey was conducted in 2010 December, using not-yet-calibrated Dutch LOFAR HBA stations (cf. Sect. 4.7 in van Haarlem et al. 2013). Initial observations used 13 core sub-stations and 4 remote stations, which increased to 38 core and 6 remote stations at the end of the survey. As remote stations are twice as sensitive as core stations, the antenna gain G for a certain LPPS configuration scales as $G \propto (n_{\rm core} + 2n_{\rm remote})/\sqrt{n_{\rm core} + n_{\rm remote}}$. As detailed in Chap. 3 of C13 these stations were combined to form sets of 7 incoherent-sum station beams (Table 1).

Full-wave electro-magnetic simulations on HBA stations (Arts et al. 2013), modeling the incoherent summation of the sets of stations used, produced the FoV listed in Table 1. The modeled LPPS beam proved well-behaved and circular in the zenith, with a full width at half maximum (FWHM) of 3.7° (Fig. 3.1 in C13). The large FoV per pointing (Table 1) allowed the survey to cover 34% of the celestial sphere (Fig. 2). Combined with

Table 1. Different observational setups used in this work.

Observation	Pointings	Beams/P	FoV/P deg^2	Res. °	t_{int} min	BW MHz	f MHz	N_{ch}	t_{samp} ms	Coh.	R_d TB/h
LPPS survey	246	7	75	3.7	57	6.8	142	560	0.655	I	0.09
LOTAS survey	206	19	3.9	0.5[a]	17	48	143	3904	1.3	C	0.8
LOTAS confirmation	–	61–217	–	<0.1	27	80	150	6576	0.49	C	12–42
LOTAS timing	–	1	–	–	15–30	80	150	6576	1.3	C	0.07

Notes. Listed are the number of pointings over the survey; the number of beams per pointing Beams/P, the field of view per pointing FoV/P, the angular resolution (FWHM of each beam), integration time t_{int}, bandwidth BW, central frequency f, number of channels N_{ch}, sampling time t_{samp}, whether beamforming was (I)ncoherent or (C)oherent, and the data rate R_d. [(a)] With the 2011 beam-former, beams at higher declinations were spaced more closely in right ascension (Sect. 4.2.1 in C13).

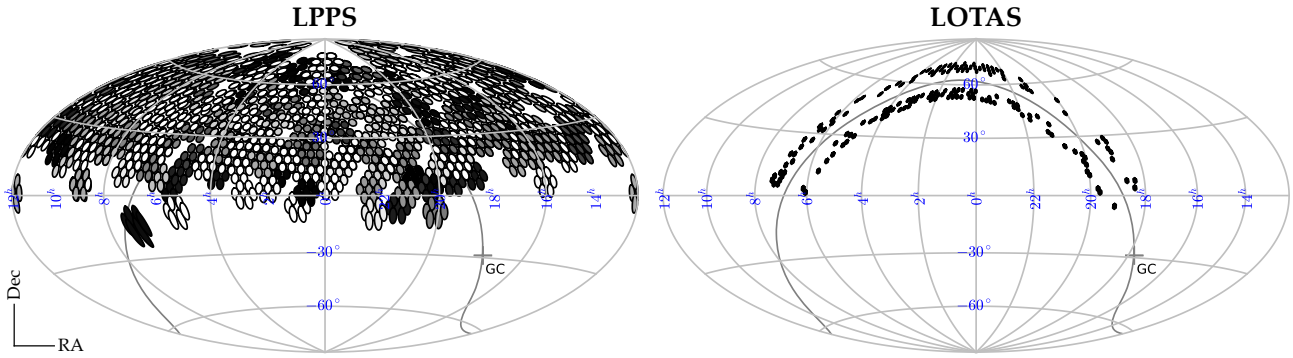

Fig. 2. Total sky coverage achieved by LPPS (*left*) and LOTAS (*right*). The Galactic plane and center are shown with a gray line and cross, respectively. The grayscale of the individual beams shows the usable observation length, where white is 0 min, and black the full 57 min for LPPS and 17 min for LOTAS.

the long dwell times, effectively up to 1 h, LPPS provided the equivalent of 9.7 min of all-sky coverage.

2.2. LOTAS survey

In May 2011 we carried out LOTAS, a tied-array survey of ~600 deg^2. By that time the 6 HBA stations on the central Superterp shared a single clock signal[1] (van Haarlem et al. 2013), which allowed for reliable tied-array beamforming (Sect. 4.2.1 in C13). This resulted in 19-beam observations covering 3.9 deg^2 per 17 min pointing (Fig. 1; Table 1). The expected tied-array beam shapes were validated through a series of characterization observations (Fig. 27 in van Haarlem et al. 2013). LOTAS sparsely surveyed two strips of sky $5° < |b| < 15°$, just off the Galactic plane, to maximize the potential for new pulsar discoveries while avoiding high scattering and background sky emission (Fig. 2).

2.3. LOTAS confirmations and timing

Confirmation observations on pulsar candidates from the LOTAS survey were performed late 2012. The availability of 24 core stations, and ability to form many tens of tied-array beams together enabled significantly higher sensitivity and angular resolution (Table 1). Confirmed candidates were timed until early 2014 with a similar but single-beam setup (Table 1).

3. Analysis

Survey data were processed to detect periodic pulsar signals and individual, dispersed bright radio bursts. This processing included data quality checks. As the implementation of this pipeline and quality control is detailed in C13, only its essentials are summarized here.

3.1. Pipeline processing

Search processing was handled by a parallelized Python pipeline, based on `PRESTO`[2] (Ransom 2001). It automated the process of radio frequency interference (RFI) excision and dedispersion (with survey specific settings, described below). It next handled periodicity searches including accounting for acceleration, single-pulse searching, as well as sifting and folding of the best candidates.

We first performed periodicity searches assuming no acceleration. Binary motion, however, can cause the intrinsically periodic signals to drift in the Fourier domain. Therefore we next performed an "acceleration" search (Ransom et al. 2002) up to a maximum number of bins, or z_{max}, of 50. For a pulsar with, e.g., a 40 ms period in a relativistic binary, LPPS is sensitive up to binary accelerations of 51 m s^{-2} (C13). We summed up to 16 harmonics, a technique where through recursive stretching and summing, the power contained in all harmonics can be recovered (Ransom 2001); and included "polishing", an extra step to reject RFI peaks acting as spurious harmonics.

The dedispersed time series were inspected for single, dispersed bursts by convolving the time series with a running box-car function and inspecting the correlation coefficient. We used box-cars 1–4, 6, 9, 14, 20 and 30 bins long, making the search sensitive to bursts between 0.655 ms and 19.5 ms at low DMs and, because of down-sampling during dedispersion, to between 41.9 ms and 1.26 s at the very highest DMs. Data that were

[1] This signal is now distributed to all 24 core stations.

[2] https://github.com/scottransom/presto

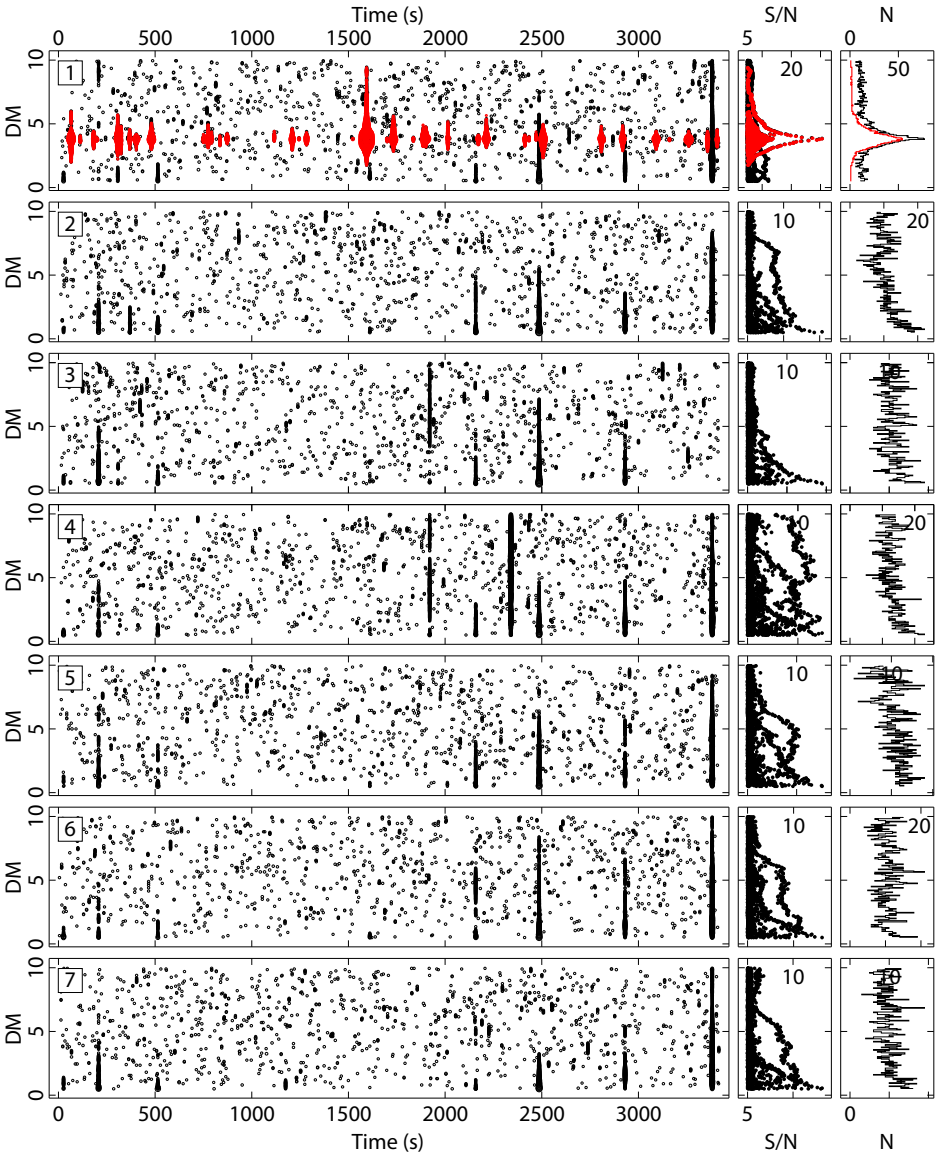

Fig. 3. A detection plot of PSR J0243+6257 (Beam 1, *top row*), as produced by our single-pulse post processing scripts. For each of the seven beams in this observation, the single-pulse detections are plotted between DMs of 0.5 cm^{-3} pc and 10 cm^{-3} pc (*left panels*). The *two right-most columns* of panels show the events collapsed in time, in DM versus cumulative (S/N) and number of events (N), respectively. The *top panel* of the plot shows PSR J0243+6257 clearly detected whilst the other beams show no detection, only some RFI. The pulsar is visible in the *main top-row* DM versus time panel as a series of individual pulses with a $DM \sim 3.9$ pc cm^{-3}. In post-processing, our automated pulse grouping algorithm (C13) has colored events that are judged to be of an astrophysical origin in red (the black points were automatically judged to be either statistical noise or RFI).

affected by RFI were discarded. For the remaining good-quality data, the PRESTO detections per individual trial-DM were next associated or "grouped" (Sect. 3.3.3 in C13) across all DMs. This freely available[3] single-pulse post-processing script looked for astrophysical signals by demanding that each single-pulse detection (or "group") had a minimum of 7 members, that it had a minimum S/N of 8 and that at least 8 such pulses occurred at roughly the same peak DM. Through trials, these numbers generally appeared to be the best heuristics to distinguish astrophysical signals from man-made ones. For each instance where these criteria were met, a plot like Fig. 3 was created for inspection. Beyond these, two-dimensional histograms of the number of detections in the time-DM plane (Fig. 3.5 in C13) were used to assess data quality and detect bright pulsars.

[3] https://github.com/tcoenen/singlepulse-search

3.1.1. LPPS

The LPPS data were reduced on the Hydra cluster at the University of Manchester. We dedispersed our data in 3487 trial-DMs up to 3000 pc cm^{-3}, and applied zero-DM filtering (Eatough et al. 2009). That technique removes all broad-band signals from $DM = 0$ pc cm^{-3}, which are assumed to be RFI. This proved useful in limiting the number of spurious single-pulse detections without negatively impacting the periodicity search results. At the lowest DMs no downsampling in time was performed and the trial-DM spacing was 0.05 pc cm^{-3}. At the very highest DMs the data were downsampled 64 times, to match the increased intra-channel dispersive smearing, and the trial-DMs are spaced in steps of 5 pc cm^{-3}. Because of this heavy downsampling in time, the high-DM part of the search added only a few percent to the total processing time.

Acceleration candidates for all 7 beams were sorted by significance, and duplicates in period and DM, across beams and across $z_{\rm max}$ values, were removed. To minimize spurious (RFI) detections, only candidates with periods 5 ms $< P <$ 15 s and $DM > 2\,{\rm pc\,cm^{-3}}$ were processed further. The `prepfold` routine from PRESTO folded each candidate and optimized in period and period derivative. Because this folding was done on the raw data, which includes frequency information, the DM could also be optimized. The resulting candidates were ranked. Two neural nets (Eatough et al. 2010), trained on the folds of LPPS pulsar re-detections and RFI instances, helped prioritize candidates.

3.1.2. LOTAS

LOTAS data were transferred from Groningen over a three-point "bandwidth-on-demand" 1−10 Gbps network, to the grid storage cluster at SURFsara[4] Amsterdam, and to Hydra. The availability of a large grid compute cluster, operated by SURFsara and part of the European grid infrastructure coordinated by EGI[5], allowed processing of the full survey data set to proceed relatively quickly. In all, the search ran on 200 8-core servers for a little over a month, for a total of 1.3 million core hours used.

For LOTAS, the DM search covered 0–1000 $\rm pc\,cm^{-3}$ with spacings increasing from 0.02–0.30 $\rm pc\,cm^{-3}$ for a total of either 16 845 or 18 100 DM trials (cf. Sect. 4.2.3 in C13). No zero-DM filtering was used. All time series were searched at the full 1.3 ms resolution.

LOTAS contained little RFI and no neural-net candidate preselection was used. We manually inspected all acceleration candidates with $\chi^2 > 2.0$. That reduced χ^2, reported by `prepfold`, is the result of fitting a straight line to the profile – noisy profiles can be fit with such a straight line and will produce low χ^2, while strong pulsars deviate and produce high χ^2. A $\chi^2 > 2.0$ corresponds to a $S/N \gtrsim 6$. We also inspected those with $1.5 < \chi^2 < 2.0$, $DM < 250\,{\rm pc\,cm^{-3}}$ and period derivative $\dot{\rm P} < 10^{-8}$ s s^{-1}. That choice of parameter space efficiently excludes RFI, which often shows large $\dot{P}$.

3.2. Telescope validation and data quality

The LPPS data were taken during LOFAR's early commissioning period and data quality issues were expected. Stations had not yet been calibrated and contained faulty initial elements that generated RFI. This affected the quality of the array beam, and a significant fraction of the data was unusable[6].

In the single-pulse search, RFI instances could sometimes overwhelm the PRESTO diagnostics. We developed a condensed version of the single-pulse diagnostic plots, where the single-pulse candidates are shown as a 2-dimensional, color-coded histogram on the time-DM plane (Chap. 5 in C13). Our removal of all 10 s blocks of data containing more than 500 single-pulse candidates considerably cleaned the LPPS data set.

We obtained a first indication of the sensitivity of this uncalibrated LOFAR setup from the sample of pulsars blindly detected in LPPS (Sect. 4.1). As detailed in Sect. 3.4.4 in C13, we extrapolated the ATNF catalog 400-MHz fluxes of this set to the LOFAR band. From an ensemble comparison to our measured S/N we found the maximum LPPS gain to be $G = 0.60 \pm 0.13$ K/Jy. That is an appreciable fraction (~40%) of LOFAR's theoretical, calibrated sensitivity.

Compared to LPPS, the LOTAS data were already found to be much cleaner of both internally generated artifacts and external RFI. This was due to both the much more mature state of the deployed stations, and the fact that the narrow, coherently formed beams are less susceptible to RFI. The wider bandwidth of LOTAS, too, helped differentiate interference – which typically peaks at $DM = 0\,{\rm pc\,cm^{-3}}$ – from pulsar signals.

4. Results and discussion

LPPS is a shallow survey that covered 34% of the sky and detected 65 known pulsars (Sect. 4.1). In Sect. 4.2, we compare this yield with a simulation of the Galactic population. LPPS also sets a stringent upper limit on the rate of low-frequency Fast Radio Bursts (Sect. 4.3). LOTAS, with its higher sensitivity, detected the first two LOFAR pulsars (Sect. 4.4).

4.1. LPPS pulsar search

The LPPS blind periodicity search yielded the re-detection of 54 pulsars. Their profiles are shown in Fig. A.1. Folding of known pulsars within the survey footprint (Sect. 4.2.4 in C13) led to the detection of a further 9. The single-pulse search resulted in 20 pulsar re-detections. This means that we were able to detect about one third of our periodicity search detections in single-pulse searches of the same data. This is in line with predictions from Stappers et al. (2011). Two pulsars, PSRs B0154+61 and B0809+74, were only detected through their individual pulses. In Table A.1 we list the detection parameters of all 65 pulsars.

The brightest pulsar in the Northern hemisphere, B0329+54, was detected in the side lobes for many observations, from up to 109 degrees away from the pointing center (Fig. 3.14 in C13).

Pulsar J2317+68 is a 813-ms pulsar at a DM of 71.158 $\rm pc\,cm^{-3}$, which we independently discovered. This source had only months earlier been discovered in the 350 MHz GBT Northern Celestial Cap (GBNCC) Survey (Stovall et al. 2014).

Pulsar J0243+6257 was discovered by the GBT350 Survey (Hessels et al. 2008, there known as J0240+62). It was detected in both the LPPS periodicity and single pulse search. In many ways this source is a prototype for the nearby, low-DM, perhaps intermittent, sources that LOFAR is best equipped to discover. The single-pulse discovery observation (Fig. 3) showed that PSR J0243+6257 has a broad pulse-energy distribution. In a 1 h follow-up observation taken with the full LOFAR HBA core and bandwidth, the large pulse-to-pulse intensity variations in PSR J0243+6257 become even more clear. In Fig. 4 we show that some bright bursts outshine the average pulse by a factor 25. In most of the well-studied pulsars this ratio is much lower (e.g., a factor of only 2 in PSR B0809+74; van Leeuwen et al. 2002). It is only higher in RRATs and PSR B0656+14 (where it is of order 100; Weltevrede et al. 2006). Using LOFAR's multi-beaming confirmation method (Sect. 2.3) this observation was also used to determine the position to RAJ = 02:42:35(3), DecJ = 62:56:5(4). With the long dwell times that can be afforded by the huge FoV of LOFAR's incoherent beam-forming mode, there are prospects for discovering other intermittent but occasionally bright sources like PSR J0243+6257.

The detection of 54 pulsars in the blind search of the LPPS data demonstrated that LOFAR is a capable pulsar search instrument. The further detection of 9 pulsars by folding on

[4] https://www.surfsara.nl/nl/systems/grid/description
[5] http://www.egi.eu/
[6] With system health monitoring now in place, the quality of current LOFAR data is much improved.

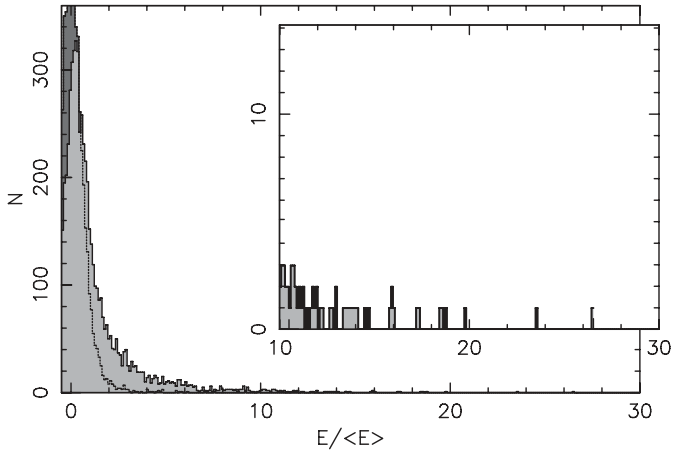

Fig. 4. Pulse energy histogram for PSR J0243+6257. Shown are the individual pulse energies for 6000 pulses, compared to their average. The dashed line, filled in dark gray, represents the off-pulse noise distribution. The light gray histogram is the energy present in the on-pulse region. That distribution peaks near zero and has significant overlap with the background histogram. In those pulses no pulsar emission is detected.

their known ephemerides means that our processing can still be improved for better extraction of pulsars from spurious, RFI-related candidates. As LOFAR now routinely produces better-calibrated, more sensitive data, the prospects for achieving a significantly deeper all-sky survey using the same incoherent beam-forming technique as LPPS is very good.

4.1.1. Comparison to recent low-frequency or wide-field surveys

Two features that make LPPS stand out from other recent pulsar survey efforts (e.g., the Parkes multi-beam pulsar survey, Manchester et al. 2001; the GBT driftscan survey, Boyles et al. 2013), are the very low observing frequency and the large dwell time. Two surveys that each *did* share one of these characteristics are the second Cambridge pulsar survey and the Allen Telescope Array (ATA) "Fly's Eye" experiment.

The second Cambridge survey at 81.5 MHz (see Shrauner et al. 1998) scanned the same northern sky as LPPS and detected 20 pulsars. The blind periodicity search of LPPS data did not detect 3 of those (B0809+74, B0943+10, B1133+16) because their LPPS pointings were corrupted. B1642−03 fell outside our survey area.

Notable features of LPPS are its large FoV, and 57-min dwell time. It shares these features with the "Fly's Eye" experiment carried out with the ATA (Welch et al. 2009) at a frequency of 1.4 GHz. Its single-pulse searches were the L-Band equivalent of those in LPPS. Down to a S/N of 8 no astronomical single pulses were detected beyond those from PSR B0329+54 (Siemion et al. 2012).

4.2. Modeling the pulsar population that underlies LPPS

On completion LPPS was the deepest large-area survey in the 100 MHz regime to date. The 65 pulsar detections constitute a low-frequency sample that is adequate in size to serve as input for a pulsar population model.

In modeling LPPS we used the dynamic, evolving model approach developed in Hartman et al. (1997). We populated the modeled Galaxy with a population of pulsars that in van Leeuwen & Stappers (2010) best reproduced the survey results of 6 large surveys. We implemented a survey model of LPPS that takes into account the total footprint on the sky, including overlapping regions (Fig. 2); the distribution of usable integration times; the sensitivity variation between pointings using different sets of stations; and the gain determined in Sect. 3.2. Based on the cumulative signal-to-noise-ratio values determined for our detected sample (Table A.1), any simulated pulsar producing a S/N over 15 was labeled detected. That S/N value is higher than the common value of 8−10 (cf. van Leeuwen & Stappers 2010) to account for the deleterious effect that RFI had on blindly identifying pulsar signals in LPPS.

In our simulation, 2.7 million pulsars formed throughout the Galaxy. Of these, 50 000 were above the death line at the present day and beamed toward Earth; 9000 are in our survey FoV. For 1200 of these, the scatter and dispersion broadening exceeds their rotational period, making them undetectable. Of the remaining 8000 pulsars, 80 are bright enough to be detected in LPPS (Fig. 5). Running the simulation over the error range on the derived gain of 0.60 ± 0.13 K/Jy produces a LPPS detected sample containing 80 ± 20 simulated pulsars. That is in reasonable agreement with the actual number of blind detections of 54. Some of the difference between these numbers could be in either the modeled survey (e.g., remaining incomplete understanding of the incoherent-addition of these commissioning era data) or the modeled population (e.g., the low-frequency spectrum turn-over behaving differently than simulated). Overall, these simulations confirm that our best pulsar population models (van Leeuwen & Stappers 2010) can accurately predict low-frequency surveys.

4.3. LPPS limit on the rate of fast radio bursts

The detection of a bright, highly dispersed radio burst of apparent extra-galactic origin was first reported by Lorimer et al. (2007) and further detections have since been reported by Keane et al. (2011), Thornton et al. (2013) and Spitler et al. (2014). As the LPPS survey provides both long dwell times and large FoV, the survey data can be used to either detect or limit FRBs at low radio frequencies.

We searched the single-pulse data (Sect. 3.1) down to a S/N of 10 at DMs between 2–3000 cm^{-3} pc. This is a much larger DM than predicted for any typical line-of-sight through our Galaxy away from the Galactic center (Cordes & Lazio 2002). Signals with such high DMs may also be highly scattered at low frequencies. Although there is an observed relation between DM and scattering delay in the Galaxy (Bhat et al. 2004), this relation has more than an order-of-magnitude scatter and any single line-of-sight may deviate significantly from the average relation. Furthermore, it is unlikely that the ionized intergalactic medium is distributed in a similar way to the Galactic interstellar medium. Such highly dispersed signals may thus continue to be detectable at LOFAR frequencies (Serylak et al. 2013; Macquart & Koay 2013; Hassall et al. 2013; Lorimer et al. 2013), making a detection possible and a limit useful.

We visually inspected all pulses that crossed this threshold of $S/N > 10$. All were associated with either a known pulsar or RFI (as evidenced by detections across multiple beams, or across multiple trial DMs with no peak in S/N) which was particularly present at low DMs. Thus, no FRBs were detected in LPPS.

For bursts that are not affected by intra-channel dispersion smearing, the resulting fast-transient limit then depends on the telescope sensitivity and the sky coverage in both time and area.

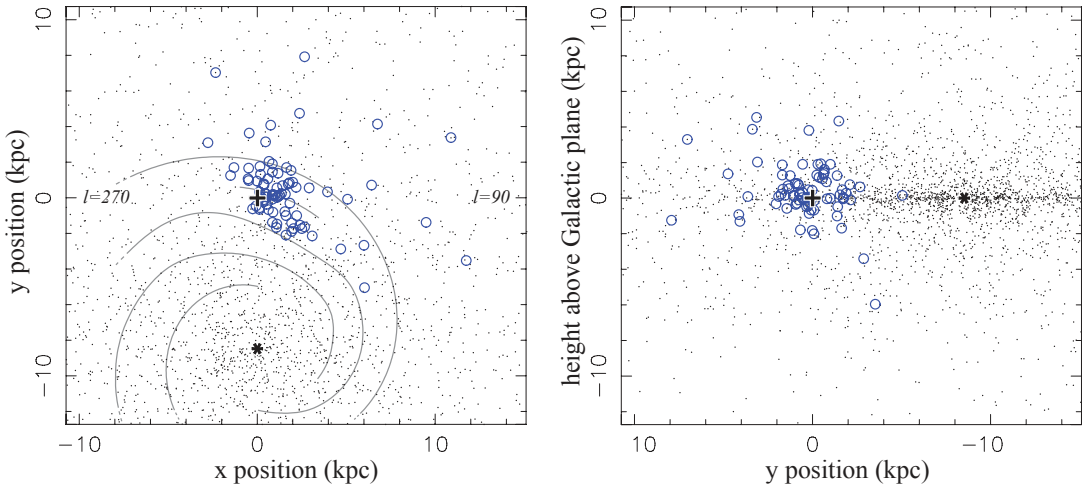

Fig. 5. Modeled pulsars in our Galaxy. Pulsars that are still emitting at the current time, and are beamed toward us, are marked with dots (only 10% of these shown). Simulated pulsars that are detected in LPPS are marked with blue open circles. The Earth is marked with a "+", the Galactic center with a "*". *Left panel*: projection onto the plane of the Galaxy is plotted, including spiral arms, with the Galactic center at $y = -8.5$ kpc from the Earth. *Right panel*: projection of the detections onto the vertical plane through the Galactic center and the Earth.

We define the sky coverage as being out to the FWHM of each beam and use the effective time coverage determined in Sect. 3.2.

We use the peak gain derived from the LPPS pulsar re-detections (Sect. 3.2) to calculate the sensitivity. For each LPPS observation this was adjusted for the number of used (sub-)stations and the zenith angle, and was multiplied by 0.73 to produce the average over the FoV. Use of the gain average, not its minimum at FWHM, is common in determining survey sensitivity (e.g., Edwards et al. 2001). Finally, we derived a flux limit for each pointing using a $T_{\rm sys} + T_{\rm sky}$ of 500 K. We removed from consideration any beam with a flux limit above 200 Jy, which was likely caused by RFI and/or calibration issues. The LPPS average flux limit is then $S_{\rm min} = 107$ Jy (Fig. 3.15 in C13).

That limit is valid when the observed burst, after dedispersion, falls within a single 0.66 ms sample. For bursts that are wider, either intrinsically or by intra-channel or step-size dispersion smearing, the burst flux is spread over a width w. The fluence $F = Sw$ is preserved when a pulse is smeared out (e.g., Thornton et al. 2013) but the sensitivity of our single-pulse searches over boxcars of up to 1.26 s (Sect. 3.1) decreases by the square root of this width w.

We thus find a rate limit R on FRBs that were detectable by LPPS of

$$R_{\rm FRB}\left(S > 107\sqrt{\frac{w}{0.66\,\mathrm{ms}}}\,\mathrm{Jy}\right) < 1.5\times10^{2}\,\mathrm{sky}^{-1}\,\mathrm{day}^{-1}. \quad (1)$$

In Fig. 6 we compare our rate to the extrapolated occurrence based on the detection of the first FRB (Lorimer et al. 2007), to the FRB rate reported in Thornton et al. (2013) and to limits set by other surveys. These other surveys were all performed at higher frequencies, 270–1400 MHz. The low observing frequency used in LPPS means that any steep spectrum sources would appear much brighter, and consequently that a flux limit obtained with LOFAR would be much more constraining when extrapolated to higher observing frequencies. The original detection of the Lorimer burst had an apparently steep spectrum (Lorimer et al. 2007), while one of the bursts reported in Thornton et al. (2013) instead showed 100-MHz-wide, bright bands. Given our limited knowledge at this time, we simply assume a flat spectral index.

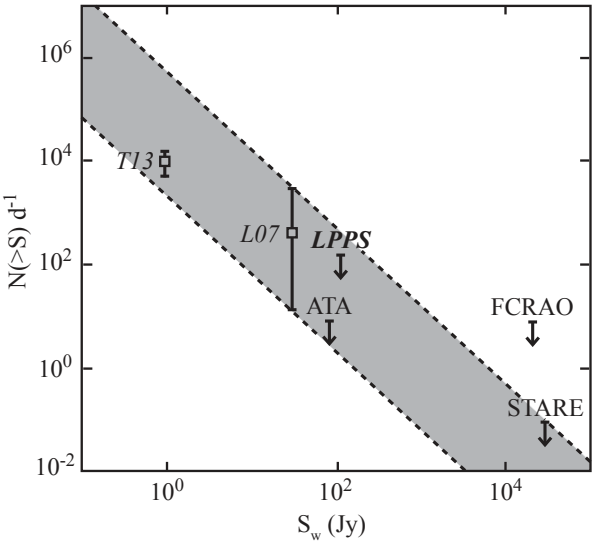

Fig. 6. Limits on transient occurrence per day N versus width-adjusted minimum flux $S_w = S/\sqrt{\frac{w}{0.66\ \mathrm{ms}}}$, on a logarithmic scale, comparing previous fast-transient surveys (Kulkarni et al. 2008) with LPPS. The burst rates reported by Lorimer et al. (2007, L07) and Thornton et al. (2013, T13) are plotted with their errors. The area between the dashed lines represents a $N(>S) \propto S^{-3/2}$ prediction from a homogeneous, stationary population of objects. The LPPS limit, which assumes a flat spectral index for the purposes of comparing with surveys at other frequencies, is seen near the center.

We can convert this celestial rate to a volumetric event frequency. We start from the assumptions that FRB emission is intrinsically shorter than our sampling time of 0.655 ms, has a luminosity at 1.3 GHz of 1 Jy Gpc^2 (Thornton et al. 2013), and follows a power-law scaling of the fluence $F(\nu) \propto \nu^{\alpha}$. We assume our intra-channel dispersion smearing dominates over scatter smearing.

For each LPPS beam we determine at which distance the decreasing flux of such an FRB falls under the minimum detectable flux for the increasingly dispersion-smeared pulse. As the distance to a simulated FRBs increases, we calculate its

flux S, which falls per the inverse-square law based on the comoving distance. At each step in redshift z, we calculate the expected DM by adding the maximum Galactic contribution in this direction (Cordes & Lazio 2002), a host contribution, and an intergalactic matter (IGM) component. We assume an intrinsic host DM of 100 pc cm^{-3} and a reduction of the effective time smearing with redshift as $1/(z+1)$. From Fig. 1 in Ioka (2003) we estimate $DM_{\rm IGM} \simeq 1100\,z$, for $z < 4$. We assume the intrinsic dispersion in the burst is negligible. From the combined effective DM we determine the number of time bins n the burst is smeared over. After also taking into account the average expected mismatch with the closest box-car length (Sect. 3.1) this results in an increase of the previously determined minimum detectable flux $S_{\rm min}$ by a factor $\sqrt{1.125n}$. The distance at which this $S_{\rm min} > S$ determines the volume this beam has searched. This is multiplied by the pointing integration time. Given our non-detection, the reciprocal of the resulting summed flux-limited volume over all such beams then produces a rate upper limit of

$$\Phi_{\rm FRB} < 2.5 \times 10^5 \left(\frac{142}{1300}\right)^{-1.3(\alpha+2)} \ {\rm Gpc^{-3}\,yr^{-1}}. \quad (2)$$

Here the dependence of the deleterious dispersion smearing on frequency causes the power-law index to deviate from the $-1.5(\alpha+2)$ expected for a purely flux-limited cosmological population. For $\alpha = -2$ our upper limit of 2.5×10^5 Gpc^{-3} yr^{-1} is higher than, and thus consistent with, the Thornton et al. FRB rate at 1.3 GHz of 2.4×10^4 Gpc^{-3} yr^{-1} as derived in Kulkarni et al. (2014). For shallower spectral indexes our rate upper limit increases further and becomes less constraining.

The limits we find are in line with those derived from other surveys. In ongoing LOFAR transient searches, we are continuing to improve on this limit and better constrain the spectra and scattering properties of such bursts. These searches will either soon detect such signals or show that the higher-frequency (∼1.4 GHz) window is ideal for their detection.

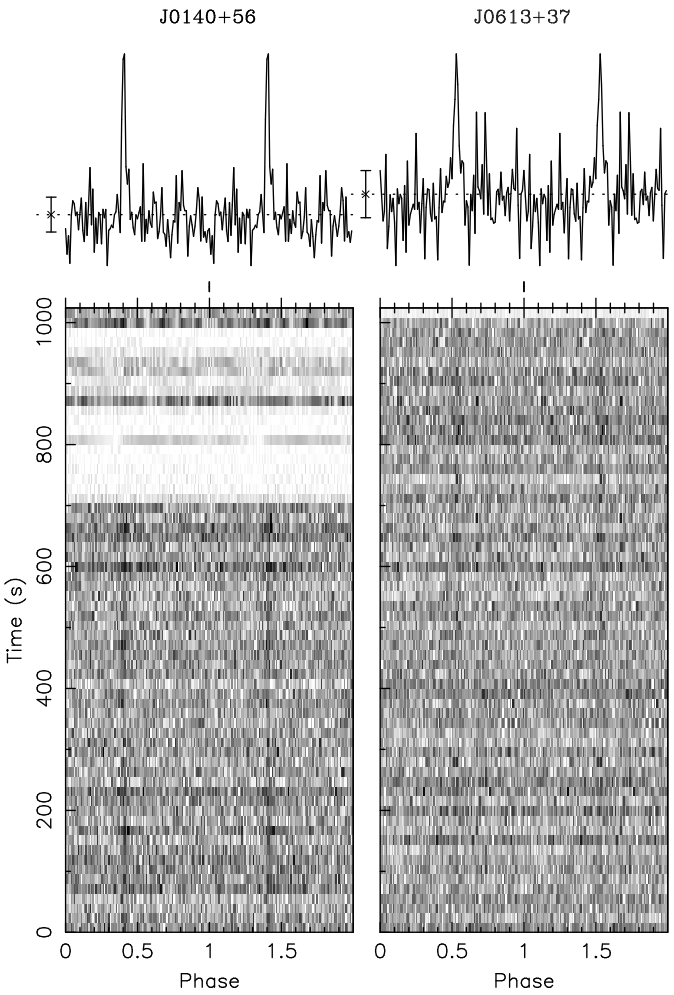

Fig. 7. Discovery plots of PSRs J0140+5622 (*left*) and J0613+3731 (*right*). *Bottom panels*: signal strength as a function of time and rotational phase. Some RFI is masked, showing up as whiteouts. *Top panels*: folded profiles, repeated twice for clarity.

4.4. LOTAS pulsar search

The LOTAS periodicity search resulted in the detection of 23 pulsars, including LOFAR's first two pulsar discoveries: PSRs J0140+5622 and J0613+3731 (Fig. 7). The parameters of all detections are listed in Table B.1. Of the 21 redetections, 17 were available in the ATNF pulsar catalog. A further four, J0216+52, J0338+66, J0358+42 and J2243+69, were independent discoveries that had only recently been found in the ongoing GBNCC survey (Stovall et al. 2014).

To judge the completeness of our blind search, we directly folded at the periods of all known pulsars within a 5-degree radius of the LOTAS pointing centers. Inspecting these folds yielded the re-detection of a further 6 pulsars. These are marked "d" in Table B.1.

The LOTAS single-pulse search output suffered from temporal misalignment between subsequent DM trials, which prevented automatic separation of astrophysical pulses from RFI. By manually inspecting the condensed plots produced by the single-pulse search (Sect. 3.2) we identified 8 bright pulsars. In Table B.1 we mark these "s" and list the S/N of the brightest pulse. We then checked for all known pulsars within a 7 degrees radius of the LOTAS pointing, but we did not detect any.

For the two discoveries, PSRs J0140+5622 and J0613+3731, confirmation and follow-up observations (Sect. 2.3) were combined to determine the rotational ephemerides. These data sets span two years. This timing analysis was performed using `PSRCHIVE` (Hotan et al. 2004; van Straten et al. 2012) and `TEMPO2` (Hobbs et al. 2006) and followed standard techniques (detailed in C13). The resulting timing solutions are given in Table 2.

When the most recent of these timing observations were carried out in 2014 January, the LOFAR sensitivity was well described and characterized, allowing for the flux measurements also listed in Table 2. As detailed in Kondratiev et al. (in prep.), these take into account e.g., the actual number of healthy dipoles used, the empirical scaling of sensitivity versus number of coherently added stations, and the exact fraction of masking due to RFI.

4.4.1. PSR J0140+5622

LOFAR's first pulsar discovery, PSR J0140+5622, has a spin period $P = 1.8$ s and $DM = 101.8$ pc cm^{-3}. Its discovery profile is shown in Fig. 7. Our timing campaign allowed us to derive a period derivative $\dot{P}$ of 7.9×10^{-14} s s^{-1}. The values derived for the characteristic age τ_c and the surface magnetic field $B_{\rm surf}$ are respectively 3.5×10^5 yr and 1.2×10^{13} G. This surface magnetic field is at the high end of the known population (Fig. 4.14 in C13). The best-fit timing model for

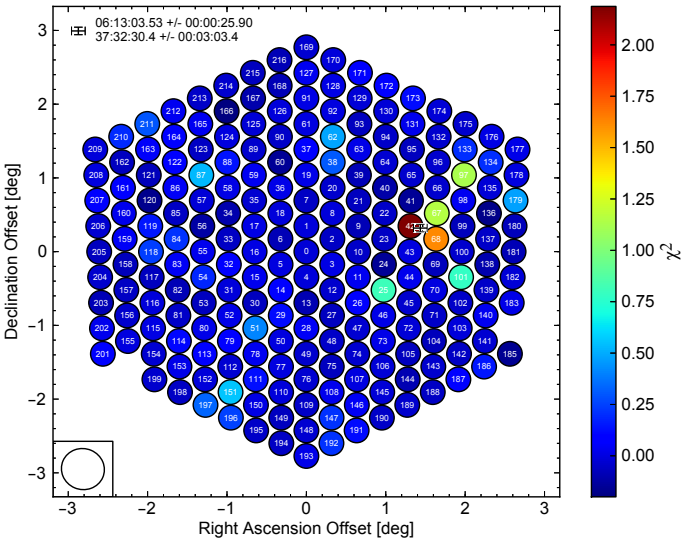

Fig. 8. Confirmation observation of PSR J0613+3731, establishing it had been discovered in a side-lobe of the original survey observation. The initially derived position was between beams 15 and 30 in this figure. Two of the 217 specified beams did not process due to a cluster hardware issue. Each beam is color coded according to the reduced chi-squared of the average pulse profile in that beam, compared to a straight line (cf. Sect. 3.1.2). The actual size of the individual tied-array beams is shown bottom left. The cross shows the pulsar's best-fit position.

PSR J0140+5622 is presented in Table 2. The estimated distance to this pulsar is 3.8 kpc, based on the NE2001 model (Cordes & Lazio 2002).

4.4.2. PSR J0613+3731

The second LOTAS pulsar discovery is PSR J0613+3731 (Fig. 7), with $P = 0.62$ s and DM = 19.0 pc cm^{-3}. While this pulsar was quickly confirmed in a multi-beam observation, its observed position appeared to vary, and it was only visible at the bottom of the observing band. Side-lobe detections of bright known pulsars showed similar behavior. As the LOTAS fractional bandwidth is large, the FWHM of a tied-array beam changes by ∼40% over the band, and the size and position of the side lobes follow. A further localization observation performed as part of the timing campaign for PSR J0613+3731, this time using 215 beams spread over an area much larger than the 19-beam footprint of a LOTAS survey observation, established the fact that PSR J0613+3731 was indeed initially discovered in a side-lobe (Fig. 8). The timing campaign along with the initial discovery and confirmation observations allowed us to derive values for $\dot{P}$, $B_{\rm surf}$ and a $\tau_{\rm c}$, which are respectively 3.2×10^{-15} s s^{-1}, 1.4×10^{12} G and 3.0×10^{6} yr. Table 2 contains the precise values for these derived quantities and also contains information about the timing solutions. The DM-derived distance to PSR J0613+3731 is 0.64 kpc.

4.4.3. Follow-up

High-frequency confirmation attempts were carried out at 1532 MHz with the Lovell telescope at Jodrell Bank Observatory. Both pulsars were ultimately detected. Pulsar J0613+3731 was seen easily, although in follow-up timing it showed considerable flux variation possibly caused by scintillation, explaining why it was missed in previous 1.4 GHz surveys. Pulsar J0613+3731 thus showcases the benefit of a low-frequency survey, where the observed bandwidth greatly exceeds the scintillation bandwidth. From a 4 h integrated profile we estimate an *L*-Band mean flux density of 0.13(6) mJy, using the radiometer equation (Eq. (3.3) in C13) to scale to the off-pulse noise. Pulsar J0140+5622 is much fainter at 1.4 GHz. Only after a total of 6 h of integration this pulsar was detected at a S/N of 10 – clearly illustrating the importance of low-frequency surveys for finding steep-spectrum sources. The resulting average flux density is listed in Table 2.

Next, both sources were weakly detected in the expected archive pointings from GBNCC (Stovall et al. 2014), by folding at their now-known periods. The resulting 350 MHz mean flux densities, derived using the radiometer equation, are listed in Table 2. Between each of the derived fluxes at 150, 350 and 1400 MHz we derived the spectral index α from a fit to $S_\nu \propto \nu^\alpha$, where S_ν is the flux density at observing frequency ν. Table 2 shows these are steeper than −2 at the low-frequency end, for both pulsars.

5. Conclusions and future work

LPPS re-detected 54 pulsars in the periodicity search, and 20, mostly overlapping, in single pulse searches. A further 9 pulsars were retrieved from the data by folding on known ephemerides (Table A.1). That detected sample agrees well with the outcome of a simulation of the Galactic pulsar population and the LOFAR telescope response. Making use of the large LPPS footprint, in both sky coverage and time, we derived a limit on the occurrence of FRBs of width w and flux density $S > 107\sqrt{\frac{w}{0.66\,\mathrm{ms}}}$ Jy of no more than 1.5×10^2 day^{-1} sky^{-1} at 142 MHz.

LOTAS produced the first two pulsars ever discovered with LOFAR. Periodicity searching also found 21 known pulsars. Of these, 8 were also re-detected through single-pulse searches. A further 6 pulsars were detected by folding data on known ephemerides.

LPPS and LOTAS were surveys in their own right – discovering new pulsars and setting the first low-frequency FRB limit. They were also critical learning steps toward a proper LOFAR pulsar survey. The full LOFAR pulsar search, the LOFAR Tied-Array All-Sky (LOTAAS, *"with double A"*) survey, includes aspects of both LPPS and LOTAS; it simultaneously creates both large incoherently formed beams and many tied-array beams using the 6 Superterp stations (Fig. 1, right panel). This setup allows the best of both worlds; the large FoV afforded through incoherent beam-forming and its concomitant sensitivity to rare bright bursts, and the raw sensitivity afforded by coherent beam-forming.

LOTAAS is using many more tied-array beams than LOTAS, as well as a much more complicated pointing strategy that takes better advantage of LOFAR's flexible multi-beaming capabilities. Each survey pointing is comprised of three sub-array pointings (i.e., three beams generated at station level). An incoherent array beam is generated for each of these sub-array pointings, and together these cover ∼60 square degrees of sky at a sensitivity roughly twice that of LPPS. Within the FoV of each incoherent beam we also form a Nyquist-sampled, hexagonal grid of 61 tied-array beams. Together, this set of 3×61 tied-array beams covers a survey area of ∼12 square degrees at a sensitivity roughly twice that of LOTAS and the GBNCC. Through 3 interlinked overlapping survey passes our sensitivity for intermittent or transient sources is greatly improved. Processing for LOTAAS has begun at the University of Manchester and on

Table 2. Measured and derived quantities for the two newly discovered pulsars.

Measured and derived quantities		
Pulsar name	J0140+5622	J0613+3732
Right ascension (J2000), α	01:39:38.561(19)	06:13:12.149(11)
Declination (J2000), δ	+56:21:36.82949(1)	+37:31:38.30520(1)
Galactic latitude, l (degrees)	129.6090	175.3357
Galactic longitude, b (degrees)	−5.8853	9.2388
Pulse frequency, ν (s^{-1})	0.56327117338(3)	1.61499182415(16)
Frequency derivative, $\dot{\nu}$ (s^{-2})	$-2.50951(8) \times 10^{-14}$	$-8.463(5) \times 10^{-15}$
Dispersion measure, DM ($cm^{-3}pc$)	101.842(32)	18.990(12)
Reference epoch (MJD)	56 000	56 000
MJD range	55 693.4−56 691.7	55 693.6−56 665.9
Number of TOAs	25	74
Rms timing residual (μs)	1151.7	996.9
Flux density at 0.15 GHz, $S_{0.15}$ (mJy)	4(1)	13(1)
Flux density at 0.35 GHz, $S_{0.35}$ (mJy)	0.7(3)	1.6(8)
Flux density at 1.4 GHz, $S_{1.4}$ (mJy)	0.02(1)	0.13(6)
Spectral index 0.15−0.35 GHz, $\alpha_{0.15-0.35}$	−2.1(1.0)	−2.5(1.3)
Spectral index 0.35−1.4 GHz, $\alpha_{0.35-1.4}$	−2.6(1.7)	−1.8(1.2)
Fractional pulse width w_{50}	0.024	0.017
Characteristic age, $\log_{10}(\tau_c$ (yr))	5.55	6.48
Surface magnetic field, $\log_{10}(B_{surf}$ (G))	13.08	12.16

Notes. Figures in parentheses are the nominal 1σ TEMPO2 uncertainties in the least-significant digits quoted. For the fluxes, errors are estimated to be 50%. The pulse widths are quoted as fraction of the pulsar period P.

the new Dutch national supercomputer Cartesius[7]. Extrapolating from the pilot surveys, LOTAAS could discover at least 200 new pulsars over the whole northern hemisphere.

5.1. The Square Kilometre Array

Looking beyond LOFAR, the two pulsar discoveries reported here are the first ever using a sparse digital aperture array. We are confident that these discoveries validate our approach to pulsar surveys, an important point as the upcoming Phase I of the Square Kilometre Array (SKA) will feature a LOFAR-like low-frequency aperture array of ∼250 000 dipole antennas (Garrett et al. 2010), more than an order-of-magnitude more collecting area than LOFAR. These will be beam-formed into stations in a LOFAR-like way. The LPPS and LOTAS surveys act as a proving ground for such flexible digital beam-forming capabilities. The techniques pioneered by LOFAR and presented here will thus be important as precursors to the eventual pulsar surveys with the SKA.

Acknowledgements. We thank J. Green and P. Abeyratne for help with LPPS processing. This work was supported by grants from the Netherlands Research School for Astronomy (NOVA3-NW3-2.3.1) and by the European Commission (FP7-PEOPLE-2007-4-3-IRG #224838) to JVL; an NWO Veni Fellowship to JWTH; and Agence Nationale de la Recherche grant ANR-09-JCJC-0001-01 to CF. LOFAR is designed and constructed by ASTRON, and is operated by the International LOFAR Telescope (ILT) foundation. LOTAS "bandwidth-on-demand" was provided by SURFnet. LOTAS processing was carried out on the Dutch grid infrastructure supported by the BiGGrid project.

Appendix A: LPPS detections and profiles

Table A.1. All pulsars detected in the LPPS data.

Pulsar	M	α (°)	DM (pc cm^{-3})	Period (ms)	S/N_p	S/N_{cum}	S/N_s
B0045+33	p	1.53	39.940	1217.0	14	–	–
B0105+65	d	1.99	30.460	1283.6	9	93	–
B0136+57*	p	2.57	73.779	272.4	7	74	–
B0138+59*	p,s	2.67	34.797	1222.9	9	29	7
B0144+59	d	1.61	40.111	196.3	7	64	–
B0154+61	s	1.37	30.00	–	–	–	9
J0243+6257	p,s	–	3.903	591.7	9	36	31
B0329+54*	p,s	2.44	26.833	714.5	606	2137	–

Notes. Sources marked with an asterisk were used to derive an estimate for the LPPS gain (see Sect. 3.2). The column headed by an M (method) lists how the pulsar was detected – through a periodicity search (p), through a direct fold using a known ephemeris (d), or through single-pulse searches (s). The next column, headed by α, lists the distance to the beam center in degrees at which the pulsar was detected (based on the ATNF pulsar database positions). The *DM* and *period* columns list the values as reported by PRESTO (without errors or digit significance) after folding the data on the known ephemeris using 256 bins. The next two columns report the *peak* and the *cumulative* S/N derived from the pulse profiles. For profiles where the off-pulse baseline is not flat (because of RFI), the signal-to-noise ratios are left blank. The last column shows the peak S/N of the brightest pulse found in the single-pulse search as reported by PRESTO (not corrected for zero-DM filtering).

[7] https://www.surfsara.nl/nl/systems/cartesius

Table A.1. continued.

Pulsar	M	α (°)	DM (pc cm^{-3})	Period (ms)	$S/N_{\rm p}$	$S/N_{\rm cum}$	$S/N_{\rm s}$
B0355+54*	p,s	1.10	57.142	156.3	32	352	7
B0402+61	p	1.65	65.303	594.5	8	82	–
B0450+55*	p	2.20	14.495	340.7	32	237	–
J0540+3207	p	–	62.371	524.2	9	–	–
B0523+11	p	0.85	79.345	345.4	7	149	–
B0611+22*	p	1.53	96.910	334.9	10	208	–
B0626+24	d	2.03	84.195	476.6	4	35	–
B0655+64*	p	0.59	8.771	195.6	81	550	–
B0809+74	s	2.66	5.75	–	-	–	14
B0823+26*	p,s	1.66	19.454	530.6	120	560	22
B0834+06*	p	1.50	12.889	1273.7	226	347	–
B0917+63	p,s	0.50	13.158	1567.9	20	243	11
B0919+06*	p	2.09	27.271	430.6	92	618	–
B0950+08*	p,s	2.23	2.958	253.0	60	658	21
B1112+50	p,s	1.68	9.195	1656.4	-	–	24
B1237+25*	p,s	1.92	9.242	1382.4	27	46	31
B1322+83	p	1.61	31.312	670.0	7	–	–
B1508+55*	p	2.10	19.613	739.6	303	1451	–
B1530+27	p,s	1.41	14.698	1124.8	–	–	10
B1541+09*	p	1.67	35.240	748.4	26	247	–
B1604−00	p	2.70	10.682	421.8	–	–	–
B1633+24	p	1.73	24.320	490.5	–	–	–
J1758+3030	p	1.33	34.900	947.2	–	–	–
B1811+40*	p	0.94	41.487	931.0	30	309	–
B1821+05*	p	1.65	66.775	752.9	25	192	–
B1839+09	p	0.75	49.107	381.3	12	–	–
B1839+56	p	2.58	26.298	1652.8	–	–	–
B1842+14*	p	1.55	41.510	375.4	29	147	-
B1905+39*	p,s	1.55	30.960	1235.7	11	38	12
B1918+26	p	0.39	27.620	785.5	18	136	–
B1919+21	p,s	2.39	12.455	1337.3	–	–	32
B1929+10	p	2.14	3.180	226.5	–	–	–
B1949+14	d	1.44	31.460	275.0	4	39	–
B1951+32	d	0.54	45.006	39.5	8	223	–
B1953+50*	p,s	1.29	31.974	518.9	28	96	12
B2016+28*	p,s	0.72	14.172	557.9	124	156	14
B2020+28*	p	0.43	24.640	343.4	50	314	–
B2021+51*	p,s	0.71	22.648	529.1	18	182	30
B2022+50*	p	1.64	33.021	372.6	9	28	–
J2043+2740*	p	1.42	21.000	96.1	22	276	–
B2110+27	p	2.95	25.113	1202.8	36	199	–
B2111+46*	p,s	1.66	141.260	1014.6	24	483	12
J2139+2242	p	0.79	44.100	1083.5	11	114	–
B2154+40	p	2.09	70.857	1525.2	–	–	–
B2217+47*	p,s	1.80	43.519	538.4	447	1976	12
B2224+65*	p	2.86	36.079	682.5	7	55	–
B2227+61	d	0.71	124.614	443.0	5	178	–
B2255+58	p	1.26	151.082	368.2	–	–	–
J2302+6028	d	2.20	156.700	1206.4	6	76	–
B2303+30	p	1.14	49.544	1575.8	–	–	–
B2306+55*	p	2.75	46.538	475.0	5	13	–
B2310+42*	p	1.78	17.276	349.4	25	215	–
B2315+21	p	2.11	20.906	1444.6	23	–	–
J2317+68	p	–	71.156	813.3	7	35	–
B2319+60	d	1.75	94.591	2256.4	2	–	–
B2334+61*	p,s	2.14	58.410	495.3	11	90	13
B2351+61	d	0.15	94.662	944.7	10	–	–

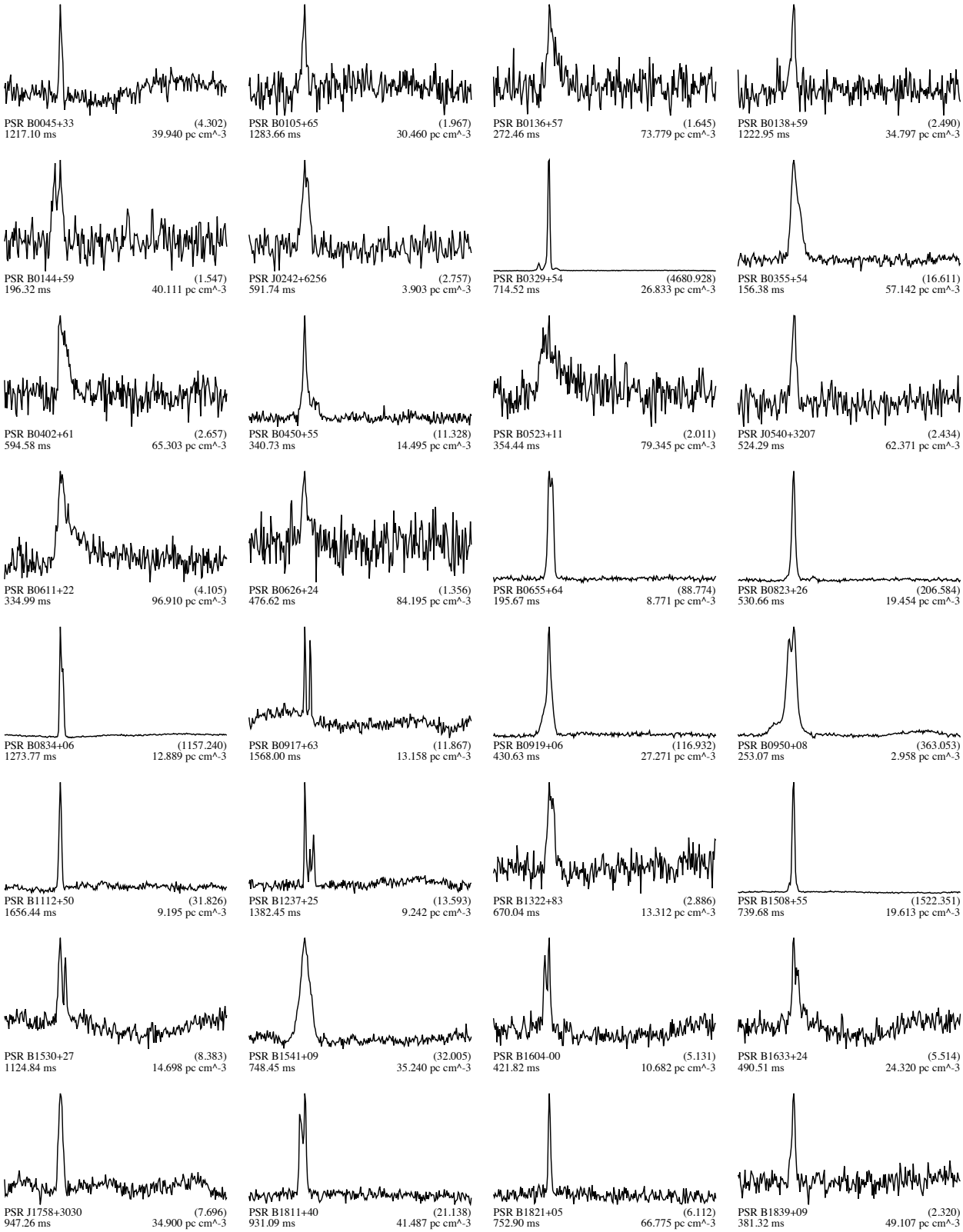

Fig. A.1. LPPS pulsar profiles. For each pulsar, the catalog name, detected pulse period, detected DM, and reduced chi-squared significance (in parentheses) from the automated search fold are given. One full rotational cycle is shown. Some of the brightest pulsars were detected multiple times; only the highest signal-to-noise detection is shown here. Several of the pulse profiles show scattering tails, e.g., PSRs B0523+11, B0611+22, B2111+46, making them excellent sources for studies of the interstellar medium. In many cases the off-pulse baseline is not flat due to RFI that could not be completely excised.

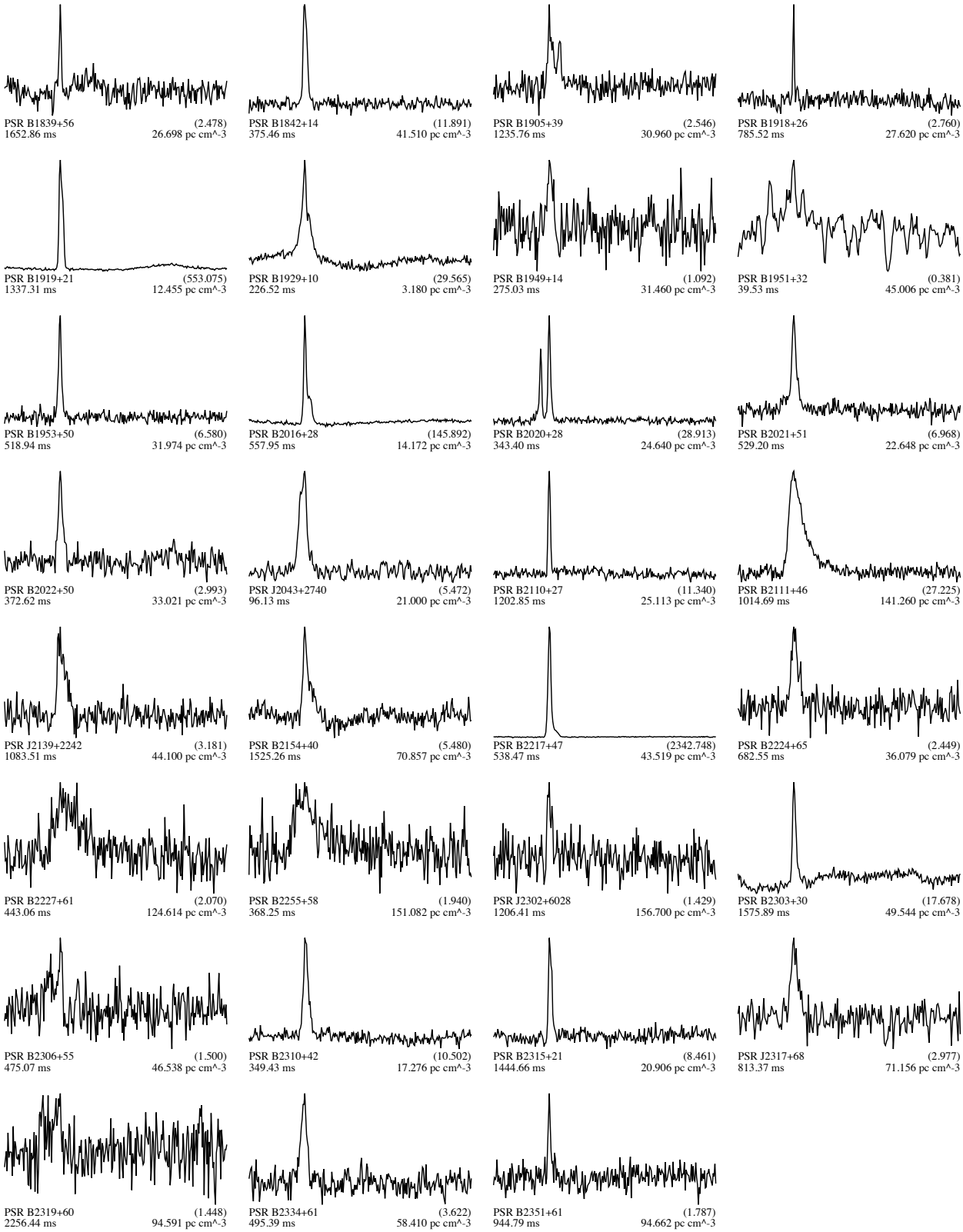

Fig. A.1. continued.

Appendix B: LOTAS detections and profiles

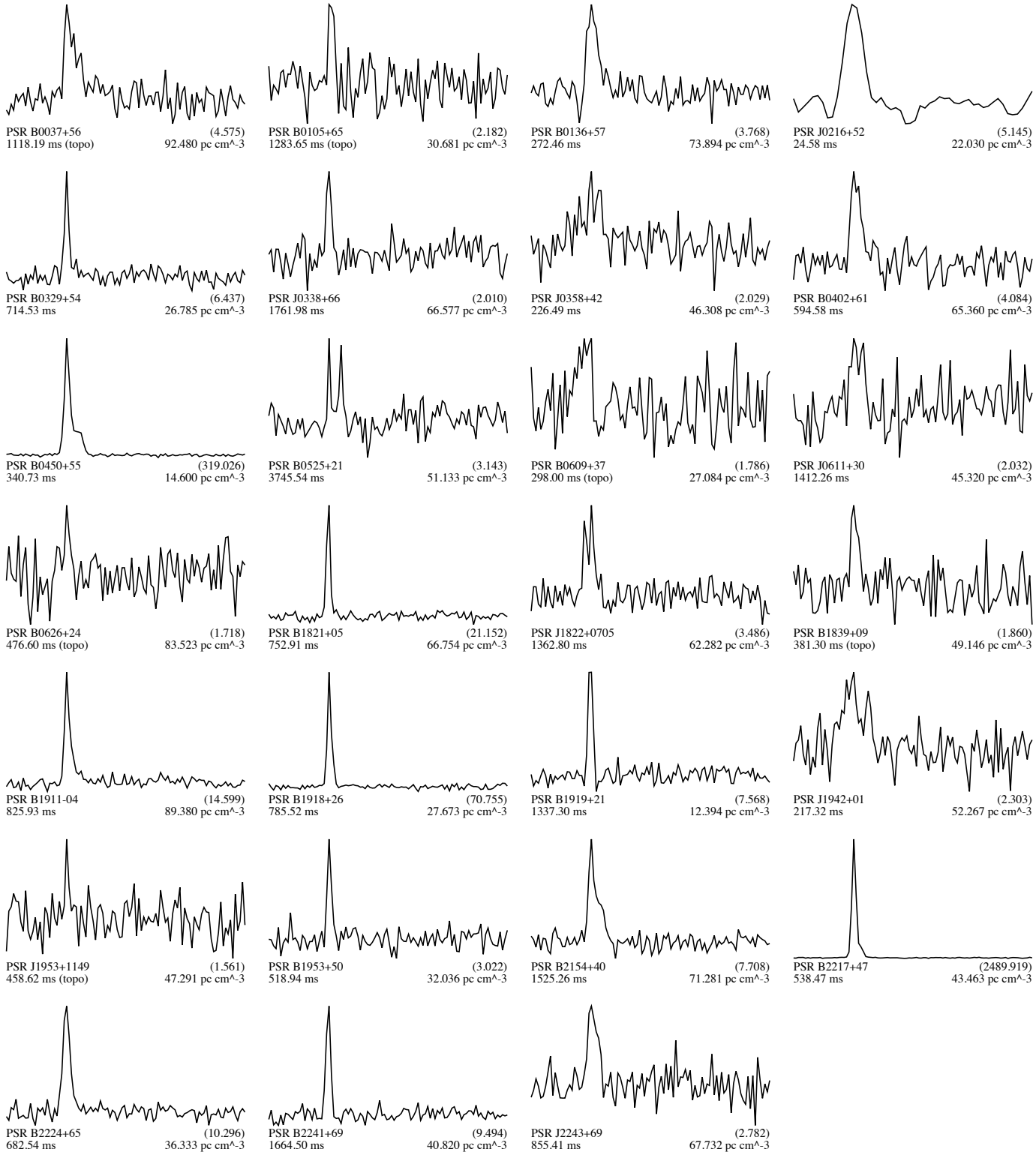

Fig. B.1. Average pulse profiles for pulsars re-detected in LOTAS. Both pulsars found in the blind periodicity search and pulsars re-detected by folding on previously known ephemerides are shown. For each pulsar the name, period, reduced chi-squared (in brackets) and DM are quoted. The reduced chi-squared is a proxy for the signal-to-noise of the pulse profile and is reported by PRESTO. Periods marked with "(topo)" are topocentric values as produced by the direct folding feature of the pipeline (Sect. 4.4).

Table B.1. A list of all LOTAS pulsar detections.

Pulsar	M	α (°)	DM (pc cm^{-3})	Period (ms)	S/N_p	S/N_{cum}	S/N_s
J0140+5622	p	0.16	101.637	1775.4	9	40	–
J0613+3731	p	1.52	19.106	619.1	5	42	–
B0037+56	d	0.19	92.480	1118.1	10	85	–
B0105+65	d	3.32	30.681	1283.6	5	22	–
B0136+57	p	3.00	73.894	272.4	9	44	–
J0216+52	p	–	22.030	24.5	20	94	–
B0329+54	p,s	4.09	26.785	714.5	19	73	10
J0338+66	p	–	66.577	1761.9	6	–	–
J0358+42	p	–	46.308	226.4	5	56	–
B0402+61	p	0.82	65.360	594.5	8	40	–
B0450+55	p,s	0.10	14.600	340.7	138	512	35
B0525+21	p,s	2.80	51.133	3745.5	9	–	17
J0611+30	p	1.95	45.320	1412.2	3	–	–
B0609+37	d	1.37	27.084	297.9	3	10	–
B0626+24	d	2.80	83.523	476.6	4	–	–
B1821+05	p,s	0.87	66.754	752.9	40	70	8
J1822+0705	p	0.20	62.282	1362.8	8	39	–
B1839+09	d	3.20	49.146	381.2	4	22	–
B1911−04	p	2.40	89.380	825.9	37	132	–
B1918+26	p,s	0.07	27.673	785.5	51	100	10
B1919+21	p	3.74	12.394	1337.2	19	26	–
J1942+01	p	0.09	52.267	217.3	5	43	–
B1953+50	p	1.29	32.036	518.9	11	6	–
J2007+0910	d	3.08	47.291	458.6	5	38	–
B2154+40	p,s	0.88	71.281	1525.2	23	68	9
B2217+47	p,s	1.45	43.463	538.4	400	913	43
B2224+65	p	2.02	36.333	682.5	23	112	–
B2241+69	p,s	0.17	40.820	1664.4	31	43	10
J2243+69	p	–	67.732	855.4	5	35	–

Notes. Pulsar names in bold are newly discovered pulsars, the first two rows contain unique LOFAR discoveries and the other pulsars with bold names signify *independent* discoveries – i.e. unpublished sources recently found by competing surveys such as the GBNCC (Stovall et al. 2014). The M column contains the method through which the pulsar was detected: (p) in the blind periodicity search, (d) through folding on a known ephemeris, and (s) by inspecting condensed single-pulse plots. The α column gives the distance to the center of the nearest tied-array beam. These distances are based on the ATNF catalog value. For the LOTAS discoveries the timing position was used. The DMs and periods quoted are taken from the PRESTO diagnostics of the folds; these values were optimized during the folding process in order to maximize the S/N. There is no error or digit significance information for these. The columns S/N_p and S/N_{cum} quote respectively the peak and cumulative S/N if they could be derived automatically. The S/N were derived from profiles with 100 bins. The S/N_s column contains the S/N of the brightest single pulse detected, possibly in another beam than the periodicity search detection.

References

Archibald, A. M., Stairs, I. H., Ransom, S. M., et al. 2009, Science, 324, 1411
Arts, M. J., Kant, G. W., & Wijnholds, S. J. 2013, SKA-ASTRON-RP-473
Backer, D. C. 2000, in Perspectives on Radio Astronomy: Science with Large Antenna Arrays, ed. M. P. van Haarlem, 285
Bassa, C. G., Patruno, A., Hessels, J. W. T., et al. 2014, MNRAS, 441, 1825
Bates, S. D., Lorimer, D. R., & Verbiest, J. P. W. 2013, MNRAS, 431, 1352
Bhat, N. D. R., Cordes, J. M., Camilo, F., Nice, D. J., & Lorimer, D. R. 2004, ApJ, 605, 759
Boyles, J., Lynch, R. S., Ransom, S. M., et al. 2013, ApJ, 763, 80
Camilo, F., Ransom, S. M., Halpern, J. P., et al. 2006, Nature, 442, 892
Coenen, T. 2013, Ph.D. Thesis, University of Amsterdam, http://dare.uva.nl/en/record/459730
Cordes, J. M., & Lazio, T. J. W. 2002 [arXiv:astro-ph/0207156]
Deneva, J. S., Stovall, K., McLaughlin, M. A., et al. 2013, ApJ, 775, 51
Eatough, R. P., Keane, E. F., & Lyne, A. G. 2009, MNRAS, 395, 410
Eatough, R. P., Molkenthin, N., Kramer, M., et al. 2010, MNRAS, 407, 2443
Eatough, R. P., Falcke, H., Karuppusamy, R., et al. 2013, Nature, 501, 391
Edwards, R. T., Bailes, M., van Straten, W., & Britton, M. C. 2001, MNRAS, 326, 358
Garrett, M. A., Cordes, J. M., Deboer, D. R., et al. 2010, in ISKAF2010 Science Meeting, The Netherlands, 18
Hartman, J. W., Bhattacharya, D., Wijers, R., & Verbunt, F. 1997, A&A, 322, 477
Hassall, T. E., Keane, E. F., & Fender, R. P. 2013, MNRAS, 436, 371
Hessels, J. W. T., Ransom, S. M., Kaspi, V. M., et al. 2008, in 40 Years of Pulsars: Millisecond Pulsars, Magnetars and More, eds. C. Bassa, Z. Wang, A. Cumming, & V. M. Kaspi, AIP Conf. Ser., 983, 613
Hewish, A., Bell, S. J., Pilkington, J. D. H., Scott, P. F., & Collins, R. A. 1968, Nature, 217, 709
Hobbs, G. B., Edwards, R. T., & Manchester, R. N. 2006, MNRAS, 369, 655
Hotan, A. W., van Straten, W., & Manchester, R. N. 2004, PASA, 21, 302
Ioka, K. 2003, ApJ, 598, L79
Janssen, G. H., Stappers, B. W., Braun, R., et al. 2009, A&A, 498, 223
Keane, E. F., Kramer, M., Lyne, A. G., Stappers, B. W., & McLaughlin, M. A. 2011, MNRAS, 415, 3065
Keane, E. F., Stappers, B. W., Kramer, M., & Lyne, A. G. 2012, MNRAS, 425, L71
Kramer, M., Lyne, A. G., O'Brien, J. T., Jordan, C. A., & Lorimer, D. R. 2006, Science, 312, 549
Kulkarni, S., Ofek, E., Juric, M., Neill, J., & Zheng, Z. 2008, http://www.astro.caltech.edu/~srk/sparker.pdf [retrieved 2010-08-19]
Kulkarni, S. R., Ofek, E. O., Neill, J. D., Zheng, Z., & Juric, M. 2014, ApJ, submitted [arXiv:1402.4766]
Lawson, K. D., Mayer, C. J., Osborne, J. L., & Parkinson, M. L. 1987, MNRAS, 225, 307
Lorimer, D. R., Bailes, M., McLaughlin, M. A., Narkevic, D. J., & Crawford, F. 2007, Science, 318, 777
Lorimer, D. R., Karastergiou, A., McLaughlin, M. A., & Johnston, S. 2013, MNRAS, 436, L5
Lorimer, D. R., & Kramer, M. 2005, Handbook of Pulsar Astronomy (Cambridge University Press)
Lynch, R. S., Boyles, J., Ransom, S. M., et al. 2013, ApJ, 763, 81
Maan, Y., Aswathappa, H. A., & Deshpande, A. A. 2012, MNRAS, 425, 2
Macquart, J.-P., & Koay, J. Y. 2013, ApJ, 776, 125
Malofeev, V. M., Malov, O. I., & Shchegoleva, N. V. 2000, Astron. Rep., 44, 436
Manchester, R. N., Lyne, A. G., Camilo, F., et al. 2001, MNRAS, 328, 17

Maron, O., Kijak, J., Kramer, M., & Wielebinski, R. 2000, A&AS, 147, 195
McLaughlin, M. A., Lyne, A. G., Lorimer, D. R., et al. 2006, Nature, 439, 817
Papitto, A., Hessels, J. W. T., Burgay, M., et al. 2013, The Astronomer's Telegram, 5069, 1
Petroff, E., van Straten, W., Johnston, S., et al. 2014, ApJ, 789, L26
Ransom, S. M. 2001, Ph.D. Thesis, Harvard University
Ransom, S. M., Eikenberry, S. S., & Middleditch, J. 2002, AJ, 124, 1788
Romein, J. W., Broekema, P. C., Mol, J. D., & van Nieuwpoort, R. V. 2010, in ACM Symposium on Principles and Practice of Parallel Programming (PPoPP'10), Bangalore, India, 169
Serylak, M., Karastergiou, A., Williams, C., et al. 2013, in IAU Symp. 291, ed. J. van Leeuwen, 492
Shrauner, J. A., Taylor, J. H., & Woan, G. 1998, ApJ, 509, 785
Siemion, A. P. V., Bower, G. C., Foster, G., et al. 2012, ApJ, 744, 109
Spitler, L. G., Cordes, J. M., Hessels, J. W. T., et al. 2014, ApJ, 790, 101
Stappers, B. W., Hessels, J. W. T., Alexov, A., et al. 2011, A&A, 530, A80
Stappers, B. W., Archibald, A. M., Hessels, J. W. T., et al. 2014, ApJ, 790, 39
Stovall, K., Lynch, R. S., Ransom, S. M., et al. 2014, ApJ, 791, 67
Thornton, D., Stappers, B., Bailes, M., et al. 2013, Science, 341, 53
van Haarlem, M. P., Wise, M. W., Gunst, A. W., et al. 2013, A&A, 556, A2
van Leeuwen, J., & Stappers, B. W. 2010, A&A, 509, A7
van Leeuwen, J., Kouwenhoven, M. L. A., Ramachandran, R., Rankin, J. M., & Stappers, B. W. 2002, A&A, 387, 169
van Straten, W., Demorest, P., & Oslowski, S. 2012, Astron. Res. Techno., 9, 237
Welch, J., Backer, D., Blitz, L., et al. 2009, IEEE Proc., 97, 1438
Weltevrede, P., Wright, G. A. E., Stappers, B. W., & Rankin, J. M. 2006, A&A, 458, 269
Zakharenko, V. V., Vasylieva, I. Y., Konovalenko, A. A., et al. 2013, MNRAS, 431, 3624

[1] Anton Pannekoek Institute for Astronomy, University of Amsterdam, Science Park 904, 1098 XH Amsterdam, The Netherlands
e-mail: leeuwen@astron.nl
[2] ASTRON, the Netherlands Institute for Radio Astronomy, Postbus 2, 7990 AA Dwingeloo, The Netherlands
[3] Jodrell Bank Center for Astrophysics, School of Physics and Astronomy, University of Manchester, Manchester M13 9PL, UK
[4] Astro Space Center of the Lebedev Physical Institute, Profsoyuznaya str. 84/32, 117997 Moscow, Russia
[5] Space Telescope Science Institute, 3700 San Martin Drive, Baltimore, MD 21218, USA
[6] School of Physics and Astronomy, University of Southampton, Southampton, SO17 1BJ, UK
[7] Department of Astrophysics/IMAPP, Radboud University Nijmegen, PO Box 9010, 6500 GL Nijmegen, The Netherlands
[8] National Centre for Radio Astrophysics, Post Bag 3, Ganeshkhind, 411 007 Pune, India
[9] Laboratoire de Physique et Chimie de l'Environnement et de l'Espace, LPC2E UMR 7328 CNRS, 45071 Orléans, France
[10] Station de Radioastronomie de Nançay, Observatoire de Paris, CNRS/INSU, 18330 Nançay, France
[11] Astrophysics, University of Oxford, Denys Wilkinson Building, Keble Road, Oxford OX1 3RH, UK
[12] Centre for Astrophysics and Supercomputing, Swinburne University of Technology, Mail H30, PO Box 218, VIC 3122, Australia
[13] ARC Centre of Excellence for All-sky Astrophysics (CAASTRO)
[14] Max-Planck-Institut für Radioastronomie, Auf dem Hügel 69, 53121 Bonn, Germany
[15] Fakultät für Physik, Universität Bielefeld, Postfach 100131, 33501 Bielefeld, Germany
[16] SURFsara, PO Box 94613, 1090 GP Amsterdam, The Netherlands
[17] Helmholtz-Zentrum Potsdam, DeutschesGeoForschungsZentrum GFZ, Department 1: Geodesy and Remote Sensing, Telegrafenberg, A17, 14473 Potsdam, Germany
[18] Leibniz-Institut für Astrophysik Potsdam (AIP), An der Sternwarte 16, 14482 Potsdam, Germany
[19] Shell Technology Center, Bangalore, India
[20] SRON Netherlands Insitute for Space Research, PO Box 800, 9700 AV Groningen, The Netherlands
[21] Kapteyn Astronomical Institute, PO Box 800, 9700 AV Groningen, The Netherlands
[22] CSIRO Australia Telescope National Facility, PO Box 76, Epping NSW 1710, Australia
[23] University of Twente, The Netherlands
[24] Harvard-Smithsonian Center for Astrophysics, 60 Garden Street, Cambridge, MA 02138, USA
[25] Institute for Astronomy, University of Edinburgh, Royal Observatory of Edinburgh, Blackford Hill, Edinburgh EH9 3HJ, UK
[26] University of Hamburg, Gojenbergsweg 112, 21029 Hamburg, Germany
[27] Research School of Astronomy and Astrophysics, Australian National University, Mt Stromlo Obs., via Cotter Road, Weston, A.C.T. 2611, Australia
[28] Max Planck Institute for Astrophysics, Karl Schwarzschild Str. 1, 85741 Garching, Germany
[29] Thüringer Landessternwarte, Sternwarte 5, 07778 Tautenburg, Germany
[30] Laboratoire Lagrange, UMR7293, Université de Nice Sophia-Antipolis, CNRS, Observatoire de la Côte d'Azur, 06300 Nice, France
[31] Leiden Observatory, Leiden University, PO Box 9513, 2300 RA Leiden, The Netherlands
[32] SmarterVision BV, Oostersingel 5, 9401 JX Assen, The Netherlands
[33] Astronomisches Institut der Ruhr-Universität Bochum, Universitaetsstrasse 150, 44780 Bochum, Germany
[34] Radio Astronomy Lab, UC Berkeley, CA, USA
[35] Sodankylä Geophysical Observatory, University of Oulu, Tähteläntie 62, 99600 Sodankylä, Finland
[36] STFC Rutherford Appleton Laboratory, Harwell Science and Innovation Campus, Didcot OX11 0QX, UK
[37] Center for Information Technology (CIT), University of Groningen, The Netherlands
[38] Centre de Recherche Astrophysique de Lyon, Observatoire de Lyon, 9 Av. Charles André, 69561 Saint Genis Laval Cedex, France
[39] Department of Physics and Elelctronics, Rhodes University, PO Box 94, 6140 Grahamstown, South Africa
[40] SKA South Africa, 3rd Floor, The Park, Park Road, 7405 Pinelands, South Africa
[41] LESIA, UMR CNRS 8109, Observatoire de Paris, 92195 Meudon, France